ChemComm

Chemical Communications

Bismuth

ROYAL SOCIETY
OF **CHEMISTRY**

COMMUNICATION
Selvan Demir *et al.*
Isolation of an organometallic yttrium bismuth cluster and
elucidation of its electronic structure

ChemComm

Check for updates

Isolation of an organometallic yttrium bismuth cluster and elucidation of its electronic structure†

Elizabeth R. Pugliese, [ID] Florian Benner [ID] and Selvan Demir [ID]*

A rare organometallic yttrium bismuth cluster complex with a heterometallocubane structure at the core was isolated and characterised by single-crystal X-ray diffraction analysis and UV-Vis spectroscopy. The anionic Bi_6^{6-} core is best described as a Zintl ion. Computational exploration of its electronic structure reveals polarised Y–Bi bonds alongside delocalisation of the Bi–Bi bonds.

The inclusion of bismuth into rare earth (RE) chemistry is exceedingly rare, with only four known metal complexes in which bismuth is immediately bound to a RE element.[1–4] Bismuth is slightly radioactive,[5] non-toxic, and possesses a large nuclear charge which evokes relativistic effects and large spin–orbit coupling.[6] These attributes lead to striking physical properties rendering bismuth compounds relevant for catalysis[7] and photovoltaic perovskite materials.[8] Our group discovered successful applications of bismuth for the design of single-molecule magnets with real magnetic memory.[2,3] Compounds containing bismuth–metal bonds are underexplored relative to other p-block elements, possibly due to enhanced reactivity. Bismuth can form higher nuclearity entities ushering in cluster formation,[9] which are known with differing topology and metal count where some follow the Zintl nomenclature. Bismuth-metal clusters bearing six bismuth atoms are particularly rare,[2,9–11] and we published the first two molecular lanthanide (Ln) bismuth cluster compounds of the formula $[K(THF)_4]_2[Cp*_2Ln_2Bi_6]$, where Cp* = pentamethylcyclopentadienyl, and Ln = Tb, Dy. Here, the core is a heterometallocubane with a Bi_6^{6-} anion bridging the two Ln(III) ions. Attaining a thorough understanding of their electronic structure and bonding situation has been impossible owing to the involved paramagnetic Ln ions and their intrinsic multiconfigurational nature. This prompted the question whether an analogous compound with yttrium ions is synthetically feasible as the slightly smaller ionic

radius of Y can cause differing products, especially under reductive synthetic conditions. Here, we report the synthesis and isolation of the first organometallic yttrium bismuth cluster compound $[K(THF)_4]_2[Cp*_2Y_2Bi_6]$ (1), featuring Bi in a chair conformation with a −6 charge. This molecule constitutes simultaneously the first dinuclear transition metal (TM) complex containing a Bi_6^{6-} core. Yttrium is innate to a stable isotope (^{89}Y) with a natural abundance of 100% and a nuclear spin of 1/2 allowing a deep insight into the electronic structure of Y compounds. Thus, 1 was characterised *via* single-crystal X-ray diffraction and density functional theory (DFT) computations. Strikingly, 1 is the only organometallic TM complex containing a metallocubane moiety.

$[K(THF)_4]_2[Cp*_2Y_2Bi_6]$ (1) was synthesised from the treatment of $Cp*_2Y(BPh_4)$ with triphenylbismuth ($BiPh_3$) in THF at room temperature followed by addition of the strong reductant potassium graphite, eqn (1). This synthetic route required development of differing reaction conditions to generate 1 relative to the procedure devised for the terbium and dysprosium analogs.[2] The addition of KC_8 allows for the reduction of the Bi^{III} present in $BiPh_3$ to Bi^{I-} in the Bi_6^{6-} cluster core. The formed byproducts are the insoluble $KBPh_4$ and graphite, alongside $Cp*_2YPh(THF)$ (2) which is readily hexane soluble, all of which can be easily separated from 1 through filtration. Black block-shaped crystals of 1 were grown from a diffusion of diethyl ether into a concentrated THF solution at −35 °C. This crystallisation method is notable as Zintl ions are typically synthesised from the mixture of alkali/alkaline earth metals and main group elements, and oftentimes necessitate the use of highly polar solvents such as ethylenediamine (en).[12] Such crystallisation conditions are not compatible with organometallic RE chemistry. Thus, we note that 1 is readily synthesised from $BiPh_3$ as the Bi source which is soluble in THF. 1 crystallises in the $P2_1/n$ space group and features a diyttrium complex that resides on a crystallographic inversion centre, such the two yttrium ions are equivalent by symmetry, Fig. 1. Each Y site is tripositive, six-coordinate, and ligated to one $Cp*^-$ ligand. The Y(III) centres are bridged by six Bi(I) ions arranged to a Bi_6^{6-} core which adopts a chair conformation reminiscent to cyclohexane. Thus, 1 constitutes the

Department of Chemistry, Michigan State University, 578 South Shaw Lane, East Lansing, Michigan 48824, USA. E-mail: sdemir@chemistry.msu.edu

(1)
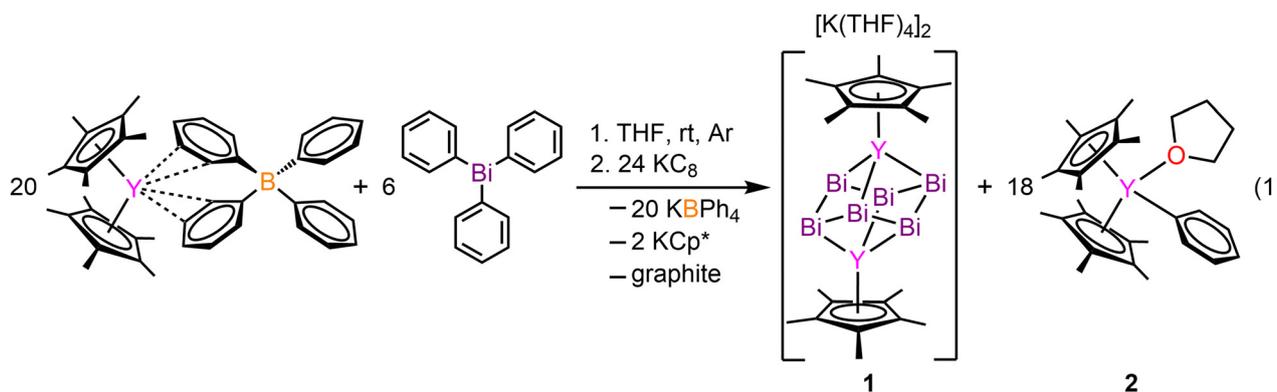
first complex of a molecular yttrium bismuth heterometallocubane. The Y–Bi distances in **1** of 3.04(2), 3.09(2), and 3.20(2) Å are in excellent agreement with intermetallic solid state compounds such as Y_5Bi_3 (3.051–3.395 Å),[13] and are similar to that of the Tb and Dy complexes.[2] The distances are shorter than 3.2335(2) Å and 3.1879(6) Å in dinuclear Y complexes containing a Bi_2^{2-} unit, $(Cp*_2Y)_2(\mu-\eta^2{:}\eta^2{-}Bi_2)$ and a Bi_2^{3-} radical, [K(crypt-222)]-$[(Cp*_2Y)_2(\mu-\eta^2{:}\eta^2{-}Bi_2^{\bullet})]\cdot2THF$,[3] respectively. This discrepancy may be attributed to the decreased steric bulk of the ancillary half-metallocene moiety.[3] The Bi–Bi distances in **1** are 3.022(9), 3.046(10), and 3.060(8) Å, suggestive of a Bi–Bi single bond (3.02 Å).[2,14] **1** constitutes the only compound comprising a 4d metal that forms a cube or a true cyclohexane conformer for Bi_6. The closest TM complex serves the icosahedral complex $[K(18-c-6)][Ni_x@\{(CO)_8Ni_6Bi_6\}]$, containing a Bi_6 unit albeit with an interstitial Ni atom and a −4 charge.[11] The average Y–Cnt distance is 2.228(22) Å, where Cnt = Cp* ring centroid, is shorter than that of the Tb (2.338(1) Å) and Dy (2.365(1) Å) congeners owing to slight differences in ionic radii.[15] Relative to other

halfmetallocene complexes such as $Cp*Y(CH_2C_6H_4NMe_2-o)_2$ the Y–Cnt bond in **1** is considerably shorter (2.390(1) Å),[16] likely due to reduced steric repulsion between the Cp* methyl groups and the Bi ions compared to the bulkier organic ligands. **1** is isostructural with the Tb and Dy homologs.[2]

UV-Vis spectra of **1** were recorded at concentrations of 20–100 µmol L^{-1} in THF at room temperature (Fig. S10, ESI†). In all cases, absorption was observed over the entire range of the visible region, never reaching absorption levels as low as a blank THF sample. Several distinguishable peaks in the visible region between 677 and 410 nm could be identified, which primarily result from transitions of occupied Bi_6^{6-}-centred orbitals to Bi_6^{6-}-centred virtual orbitals as confirmed via TDDFT calculations (Table S7, ESI†). Notably, excitations into the two near-degenerate lowest-lying unoccupied $\pi*$ orbitals are of negligible importance for transitions above 420 nm.

Excitingly, **1** allows for the first-time a thorough analysis of the electronic structure of bismuth clusters in the vicinity of organometallic RE scaffolds, due to the diamagnetic Y ions. In addition, their most stable +III oxidation state precludes ambiguities regarding the Bi oxidation state, which often cannot be assigned in Zintl clusters based on TM.[9] To this end, we performed quantum chemical calculations via DFT methods, and the obtained electron density was analysed via natural localised molecular orbitals (NLMOs), nucleus independent chemical shift (NICS) and Bader's quantum theory of atoms in molecules (QTAIM).

The calculated frontier orbitals reveal that the highest occupied orbitals (HOMO−2–HOMO) involve Y and Bi_6^{6-} contributions (Fig. 2), while the low-lying unoccupied orbitals (HOMO+1–HOMO+3) are primarily Bi_6^{6-} centred (Fig. 2). Noticeably, the HOMO features a π-bonding symmetry, a feature indicative of metal φ- or σ-aromatic systems.[9,10]

NLMO localisation of the canonical orbitals provide further insight into the bonding situation. For every Bi atom two bonding interactions to neighbouring Bi atoms were observed, which are primarily of 6p character with minor contributions from the Y atoms (∼6%) (Fig. 2). Each Bi atom partakes in one Y–Bi bond, which is strongly polarised towards the Bi atoms (∼78% Bi and ∼18% Y contribution) with ∼16% s-/∼83% p-hybridisation in Bi and ∼37% s-/∼62% d-hybridisation in Y. In addition, each Bi atom features one lone pair (LP) of primary s-character (Fig. 2). Although all bonds appear to be localised
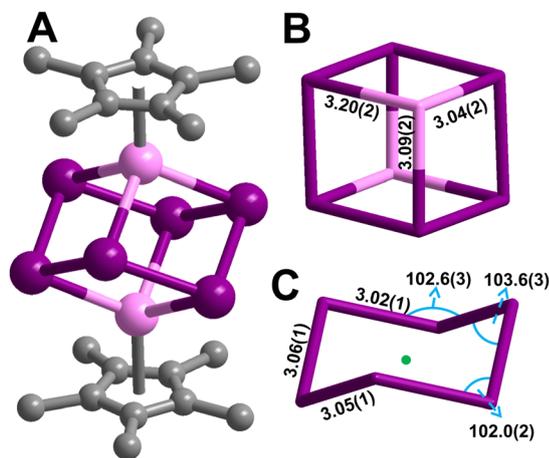

Fig. 1 (A) Structure of $[K(THF)_4]_2[Cp*_2Y_2Bi_6]$ (**1**). Pink, purple, and grey spheres represent Y, Bi, and C atoms, respectively. H atoms and both $[K(THF)_4]^+$ cations have been omitted for clarity. (B) Neutral $\{Y_2Bi_6\}$ cube enlarged with Y–Bi distances labelled. (C) Bi_6^{6-} chair enlarged with distances and angles labelled. The green mark represents the inversion centre. All distances (Å) and angles (°) are rounded up for clarity and full values are in the main text.
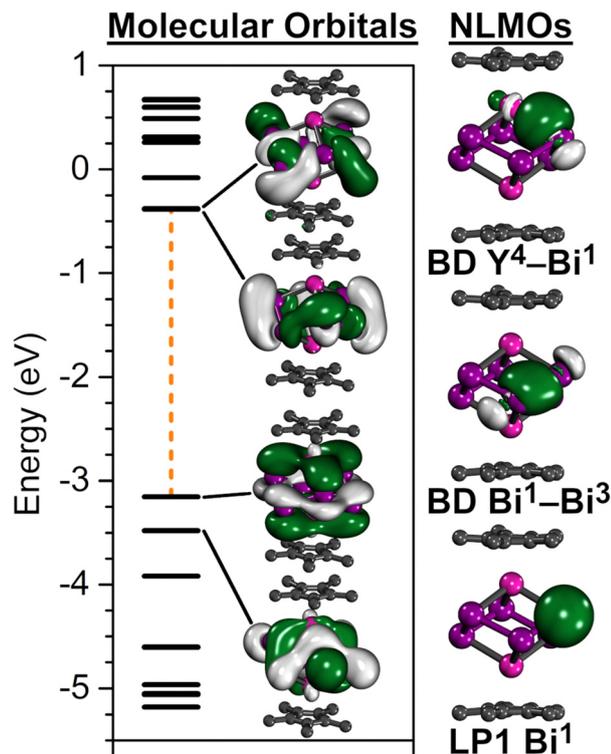
Fig. 2 Left: Energy diagram of the 10 highest occupied and 10 lowest unoccupied orbitals with graphic depiction of the respective two highest occupied and lowest unoccupied frontier orbitals. The orange dashed line highlights the HOMO−LUMO gap (3.14 eV). Right: Depiction of selected representative natural localised molecular orbitals (NLMO) illustrating a strongly polarised Y−Bi interaction (top), a Bi−Bi interaction through 6p orbitals (middle), and a Bi lone pair (bottom).

within the cluster, a small degree of electron delocalisation is indicated *via* the occupation difference between NBO and NLMO, where the LP NBOs exhibit slightly decreased occupancies of 1.93. This is also reflected within the second order perturbation analysis, where the Bi LPs are donating into vacant Y d-orbitals as well as antibonding Y−Bi and Bi−Bi bonds (Table S5, ESI†).

The electron localisation function (ELF) serves as a visualisation tool for the probability to localise an electron pair within a given spatial extent. ELF values range between 0 and 1, where 1 represents ideal localisation, 0.5 corresponds to electron-gas like probability, and <0.5 indicates delocalisation in low-density regions.[17] The ELF for **1** shows interacting electrons between neighbouring Bi atoms are delocalised, while the LPs are localised and visible as outward-facing clouds (Fig. 3 and Fig. S7, ESI†). This can be correlated to the cluster interacting weakly with two $[K(THF)_4]^+$ cations in the solid state where K···Bi = 3.9 (2) Å (Fig S4, ESI†). Lastly, the highly ionic nature of the Y−Bi interactions are visible as gaps between the Bi and Y atoms.

Bi atoms in close proximity, *i.e.* positioned in a prismatic array, may feature substantial ϕ aromaticity.[9] The Bi$_6$ assembly in **1** is peerless and potentially aromatic. To probe this, the powerful method NICS was chosen as a phenomenological descriptor for the aromatic shielding/deshielding. NICS values

were calculated along the axial (through Cnt–Y bonds) and equatorial (through opposing Bi atoms) axis (Fig. S8, ESI†). The obtained values were plotted against the distance in Å from the cluster core (Fig. S8, ESI†). The NICS0 value (centre of the cluster) is negative (δ_{NICS0} = −7.77 ppm), which at first glance suggests a diatropic ring current and aromaticity. Relative to other metal aromatic systems, this value is much smaller; for example $[K(crypt-222)][\{CpRu\}_3Bi_6]$ exhibits δ_{NICS0} = −21.3 ppm,[9] and $[Re_2(CO)_8(\mu\text{-BiPh})_2]$ δ_{NICS0} = −37.8/−41.78 ppm.[18] The equatorial NICS profile reveals progressively negative NICS when approaching the Bi atoms. Conversely, traversing the axial direction yields positive NICS values between ±1.25 and 2.25 Å near the Y atoms, before adopting negative values close to the aromatic Cp rings again. A planar, organic, and aromatic compound exhibits a gradual NICS profile,[18,19] which is only seen close to the cluster centre (∼±1 Å) before contributions from either Y or Bi dominate the NICS values. Hence, the slight deshielding observed at the NICS0 position likely arises from the proximity of the Bi⁻ ligands and their large ionic radii rather than a true ring current and associated metal aromaticity (see space filing model in Fig. S2, ESI†). The Bi_6^{6-} chair was also calculated without the $\{Cp^*Y\}^{2+}$ fragments for comparison (Fig. S9, ESI†). Here, the NICS0 and values perpendicular to the chair are positive, indicative of antiaromaticity. Hence, the highly Lewis acidic half-metallocene moieties affect the electronic structure of the Bi_6^{6-} chair, due to the vicinity of the cluster core and the Y centre (2.146 Å).

The electronic structure analysis of **1** *via* QTAIM visualises first the Laplacian of the electron density ($\nabla^2\rho$) which proves the highly ionic bonding suggested *via* NLMO investigation (Fig. 3). The real space values at bond critical points (bcp) show that all bonding interactions within the $[Y_2Bi_6]^{2-}$ cluster fall within the range of intermediate bonding regime between ideal covalent and ionic bonding, best exemplified by the slightly positive $\nabla^2\rho$ and slightly negative $H(r)$ values and negative $H(r)/\rho$ ratios. The ellipticity of the electron density $\varepsilon(r)$ is near 0 for each bond, further hinting at single bonds in the cluster moiety. The lack of electron delocalisation is reflected in the curvature of electron density perpendicular to the ring critical points (RCPs, $\lambda_{\pi3}$) of the cubane faces, which is two orders of magnitude smaller than the value found for benzene.[20,21] The associated Mayer bond indices (MBOs) clarify the bond strengths, where values ∼1 are calculated for each Bi−Bi bond and ∼0.5 for each Y−Bi bond.

In conclusion, the first heterometallocubane complex, $[K(THF)_4]_2[Cp^*_2Y_2Bi_6]$, **1**, containing a Bi_6^{6-} cluster and a transition metal was isolated, wherein the bismuth core bridges two $\{Cp^*Y\}^{2+}$ fragments and the hexabismuth moiety features a chair-like conformation akin to cyclohexane. Computational bonding analysis of **1** revealed polarised Y−Bi bonds and delocalised electrons within the Bi−Bi bonds. NICS calculations uncovered potential diatropic ring current, which however is ascribed to the proximity of the large Bi ions, rather than reflecting an authentic ring current. Notably, analysis of the bismuth chair alone reveals a paratropic ring current, which implies that the Y^{III} centres alter the electronic structure of the
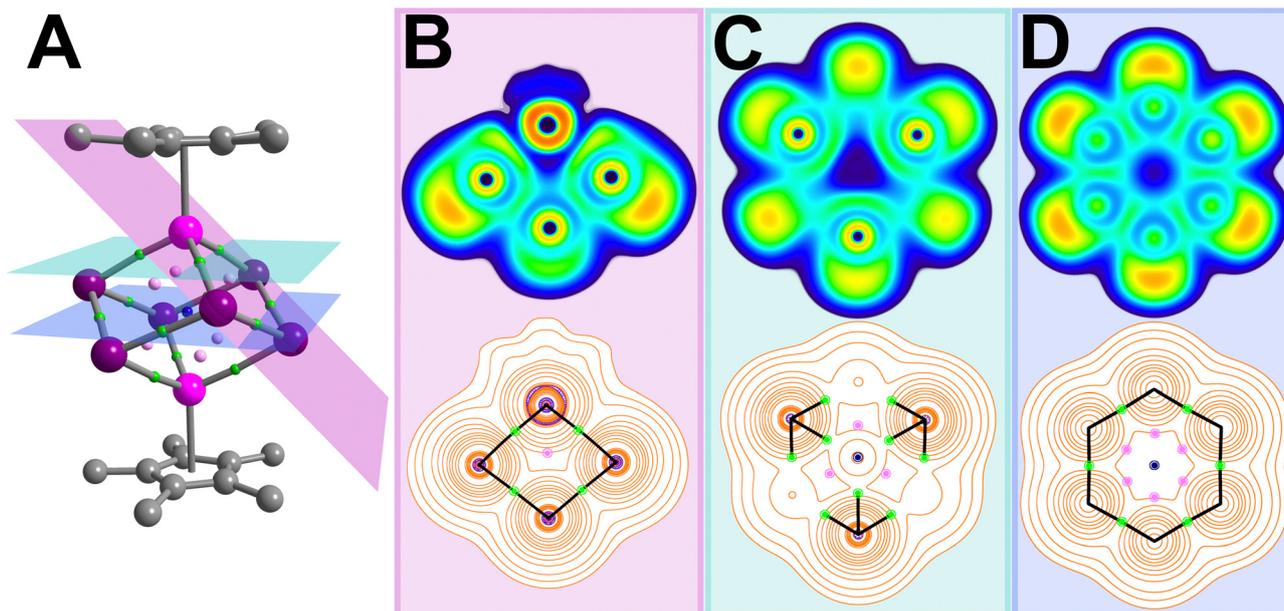
Fig. 3 Results of the QTAIM analysis of **1**, where large pink, purple, grey spheres represent Y, Bi and C atoms, and small pale pink, green and blue spheres represent bond critical (BCP), ring critical (RCP) and cage critical points (CCP), respectively (A). The electron localization function (ELF, top) and Laplacian of the electron density (bottom) are plotted along the pink, green and blue planes through the inner-cluster BCPs (B–D). ELF values are defined between 0 (dark blue) and 1 (red) to map electron pair probability within a spatial region, where a value of 1 represents ideal localisation and 0.5 (green) correspond to electron-gas like probability, while values <0.5 indicate delocalisation in low-density regions. In the Laplacian plots, orange and purple contour lines correlate with charge depletion and accumulation, and black lines represent bond paths connecting neighbouring Bi and Y atoms, respectively. In (B) contributions from the Cp* ligand were omitted for clarity. Real space values at all critical points are listed in Table S6 (ESI†).

cluster core significantly. These foregoing results are crucial for a thorough understanding of currently underexplored RE-Bi complexes, which are relevant for SMM design and potentially other future applications such as in small molecule activation.

Conflicts of interest

There are no conflicts to declare.

Notes and references

1   W. J. Evans, S. L. Gonzales and J. W. Ziller, *J. Am. Chem. Soc.*, 1991, **113**, 1589–1591.
2   P. Zhang, F. Benner, N. F. Chilton and S. Demir, *Chem*, 2022, **8**, 717–730.
3   P. Zhang, R. Nabi, J. K. Staab, N. F. Chilton and S. Demir, *J. Am. Chem. Soc.*, 2023, **145**, 9152–9163.
4   E. R. Pugliese, F. Benner and S. Demir, *Chem. – Eur. J.*, 2023, DOI: **10.1002/chem.202302687**.
5   P. De Marcillac, N. Coron, G. Dambier, J. Leblanc and J. P. Moalic, *Nature*, 2003, **422**, 876–878.
6   P. Pyykko, *Chem. Rev.*, 1988, **88**, 563–594.
7   H. W. Moon and J. Cornella, *ACS Catal.*, 2022, **12**, 1382–1393.
8   L. Zhang, K. Wang and B. Zou, *ChemSusChem*, 2019, **12**, 1612–1630.
9   B. Peerless, A. Schmidt, Y. J. Franzke and S. Dehnen, *Nat. Chem.*, 2023, **15**, 347–356.
10 L. Qiao, D. Chen, J. Zhu, A. Muñoz-Castro and Z. M. Sun, *Chem. Commun.*, 2021, **57**, 3656–3659.
11 J. M. Goicoechea, M. W. Hull and S. C. Sevov, *J. Am. Chem. Soc.*, 2007, **129**, 7885–7893.
12 K. Beuthert, B. Peerless and S. Dehnen, *Commun. Chem.*, 2023, **6**, 109.
13 B. C. Wang, E. J. Gabe, L. D. Calvert and J. B. Taylor, *Acta Crystallogr., Sect. B: Struct. Crystallogr. Cryst. Chem.*, 1976, **32**, 1440–1445.
14 L. Pauling, *The Nature of the Chemical Bond*, Cornell University Press, 3rd edn, 1960.
15 R. D. Shannon, *Acta Crystallogr., Sect. A*, 1976, **32**, 751–767.
16 T. Shima, M. Nishiura and Z. Hou, *Organometallics*, 2011, **30**, 2513–2524.
17 A. D. Becke and K. E. Edgecombe, *J. Chem. Phys.*, 1990, **92**, 5397–5403.
18 E. Schott, X. Zárate and R. Arratia-Pérez, *Polyhedron*, 2011, **30**, 846–850.
19 E. R. Pugliese, F. Benner, E. Castellanos, F. Delano and S. Demir, *Inorg. Chem.*, 2022, **61**, 2444–2454.
20 S. T. Howard and T. M. Krygowski, *Can. J. Chem.*, 1997, **75**, 1174–1181.
21 N. A. Da Silva, R. E. Bruns and R. L. A. Haiduke, *J. Phys. Org. Chem.*, 2021, **34**, 1–12.